We are IntechOpen, the world's leading publisher of Open Access books Built by scientists, for scientists

4,800
Open access books available

122,000
International authors and editors

135M
Downloads

Our authors are among the

154
Countries delivered to

TOP 1%
most cited scientists

12.2%
Contributors from top 500 universities

CLARIVATE ANALYTICS BOOK CITATION INDEX INDEXED

WEB OF SCIENCE™

Selection of our books indexed in the Book Citation Index in Web of Science™ Core Collection (BKCI)

Interested in publishing with us?
Contact book.department@intechopen.com

Numbers displayed above are based on latest data collected.
For more information visit www.intechopen.com

Chapter 9

Nanometer Structured Epitaxial Films and Foliated Layers Based on Bismuth and Antimony Chalcogenides with Topological Surface States

Lidia N. Lukyanova, Yuri A. Boikov, Oleg A. Usov, Mikhail P. Volkov and Viacheslav A. Danilov

Additional information is available at the end of the chapter

http://dx.doi.org/10.5772/65750

Abstract

The thermoelectric and galvanomagnetic properties of nanometer structured epitaxial films and foliated layers based on bismuth and antimony chalcogenides were investigated, and an increase in the figure of merit Z up to 3.85×10^{-3} K^{-1} was observed in the $Bi_{0.5}Sb_{1.5}Te_3$ films over the temperature range of 180–200 K. It is shown that an increase in the Seebeck coefficient and the change in the slope on temperature, associated with changes in the effective scattering parameter of charge carriers and strong anisotropy of scattering in the films, lead to enhance power factor due to the growth of the effective mass of the density of states. These features are consistent with the results of research of oscillation effects in strong magnetic fields at low temperatures and research of Raman scattering at normal and high pressures in the foliated layers of solid solutions $(Bi, Sb)_2(Te, Se)_3$, in which the topological Dirac surface states were observed. The unique properties of topological surface states in the investigated films and layers make topological insulators promising material for innovation nanostructured thermoelectrics.

Keywords: thermoelectric films, topological surface states, power factor, scattering on interphase, block boundaries

1. Introduction

Thermoelectrics based on bismuth and antimony chalcogenides are well known and have been extensively studied for their excellent thermoelectric properties [1–3]. Recently, the nanostruc-

tured $(Bi,Sb)_2(Te,Se)_3$ epitaxial films were shown to possess an enhanced thermoelectric figure of merit Z compared to corresponding bulk crystals due to mechanical stresses and intensive phonon scattering at the grain boundaries. Lattice thermal conductivity of heteroepitaxial nanostructured films may be substantially diminished, as compared to corresponding bulk crystals, due to acoustic phonon scattering by grain and interface boundaries. Boundaries and strain may be easily induced in thin Bi_2Te_3-based films grown on mismatched substrates. In contrast to point defects, which suppress heat transfer by short wave phonons, grain and interface boundaries are efficient in scattering of long wave ones. That is why, investigation of thin films with different structure and level of mechanical stresses looks quite important for development of thermoelectric materials with enhanced performance.

At the current stage, a new property of these materials, known as topological insulator, became one of the important subjects of the investigations [4–6]. These novel quantum states are the result of the electronic band inversion due to strong spin-orbit interaction, so the bulk becomes insulating and the surface displays an unusual metallic electronic surface state of Dirac fermions with linear dispersion and spin texture that ensures high mobility of charge carriers due to the lack of backscattering on defects. The nanostructured films of topological materials [7, 8] theoretically proved the possibility of formation of topological excitons that can condense in a wide temperature range with the appearance of superfluidity and thus a significant increase in the mobility of the charge carriers. Currently, there is only a preliminary report on the pilot study of the heterostructure Sb_2Te_3/Bi_2Te_3, which assumes the realization of exciton condensation [9]. The theoretical model [10] for topological thermoelectrics based on the Landauer transport theory shows that the value of the Seebeck coefficient and thermoelectric efficiency is determined by the ratio of the mean free path of Dirac fermions to the mean free path of bulk electrons. According to the proposed model, an increase in the contribution of the surface states and the energy dependence of the lifetime of the electronic states provide the maximum amount of the Seebeck coefficient and the increase in the thermoelectric efficiency. Experimental research of transport of thin films $(Bi_{1-x}Sb_x)_2Te_3$ [11] carried out in a wide range of compositions, and temperatures have confirmed validity of this model. It follows that the study of surface states of Dirac fermions is promising for thermoelectricity to improve the energy conversion efficiency of nanostructured thermoelectrics. This chapter includes the thermoelectric properties under normal conditions and under high pressure, galvanomagnetic and optical properties of nanostructured films based on Bi_2Te_3, obtained by different methods, in order to determine the possible effect of the topological surface states of Dirac fermions depending on the composition, the Seebeck coefficient and temperature.

2. Features of formation and structure of the grown $(Bi,Sb)_2Te_3$ films

Because of incongruent evaporation/sublimation of $(Bi,Sb)_2Te_3$ solid solutions and pronounced volatility of tellurium at temperatures higher than 400°C, formation of stoichiometric epitaxial films of bismuth and antimony chalcogenides is a nontrivial task. Hot wall technique [12, 13] was used to grow stoichiometric $Bi_{0.5}Sb_{1.5}Te_3$ layers with a thickness of 30–500 nm.

http://dx.doi.org/10.5772/65750

Structure of the grown thermoelectric films was investigated by X-ray (Philips X'pert MRD, $CuK_{\alpha 1}$, $\omega/2\Theta$- and ϕ-scans). Surface morphology of the grown $(Bi,Sb)_2Te_3$ films was studied by atomic force microscopy (Nanoscope IIIa, tipping mode). Nanostructured epitaxial thermoelectric films of $(Bi,Sb)_2Te_3$ were grown by hot wall technique on mica (muscovite) substrates. Usage of a mica substrate promotes small in-plane misorientation of the blocks in the BST film, but relatively high deposition temperature is in a favor of low density of defects in their volume. Thickness of the grown thermoelectric layers was in the range of 30–500 nm. Substrate temperature during thermoelectric film formation was roughly 70°C less then temperature of sublimating stoichiometric $Bi_{0.5}Sb_{1.5}Te_3$ burden. X-ray $\omega/2\Theta$ scans were traced for the grown $Bi_{0.5}Sb_{1.5}Te_3$ films when plane including incident and reflected Roentgen beams was in plane normal to (000.1) of mica or (10$\underline{1}$.5) of the thermoelectric layer (see **Figures 1** and **2**). From obtained scans follow that c-axis in the $(Bi,Sb)_2Te_3$ films grown on mica by hot wall technique was normal to substrate plane. Driving force for preferential orientation of c-axis in the grown films along normal to a substrate plane was substantial anisotropy of a surface free energy of the bismuth and antimony chalcogenides. From X-ray, ϕ-scan traced for a (10$\underline{1}$.5) $Bi_{0.5}Sb_{1.5}Te_3$ reflex, see insert in **Figure 1**, follows that thermoelectric films grown on mica were well in-plane preferentially oriented as well. In-plane disorientation of blocks in the films was ~0.3°. (The estimation obtained from full width at half of a maximum of a peak on the ϕ-scan. Roughly, equidistant system of growth steps was clear detectable at the film surface (see **Figure 2**), at AFM image of free surface of the $(Bi,Sb)_2Te_3$ film grow on mica. Height of the growth steps was about 1 nm.

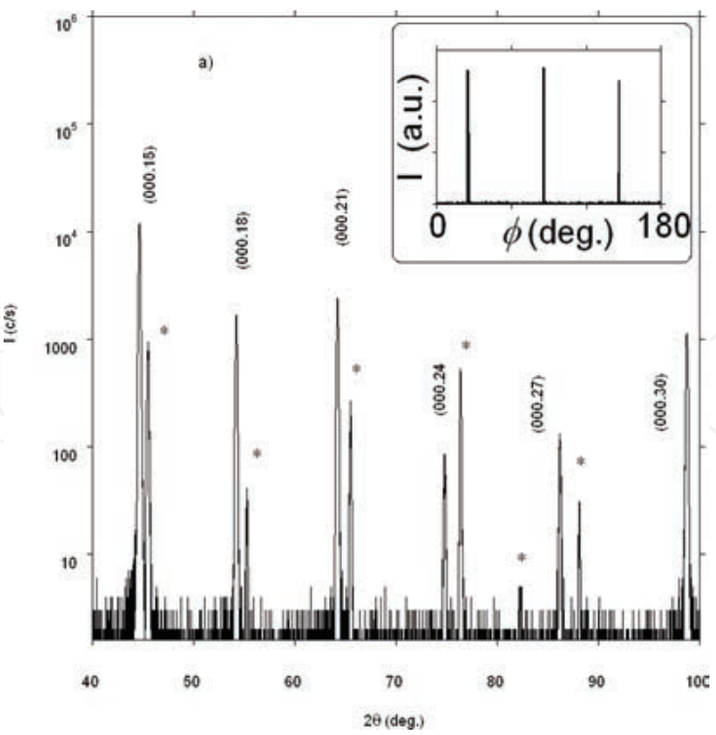

Figure 1. X-ray $\omega/2\Theta$ scan traced for the grown $Bi_{0.5}Sb_{1.5}Te_3$ film when plane including incident and reflected Roentgen beams was in plane normal to (000.1) plane of substrate. Insert plots ϕ-scan of a (10$\underline{1}$.5) reflex from the same film.

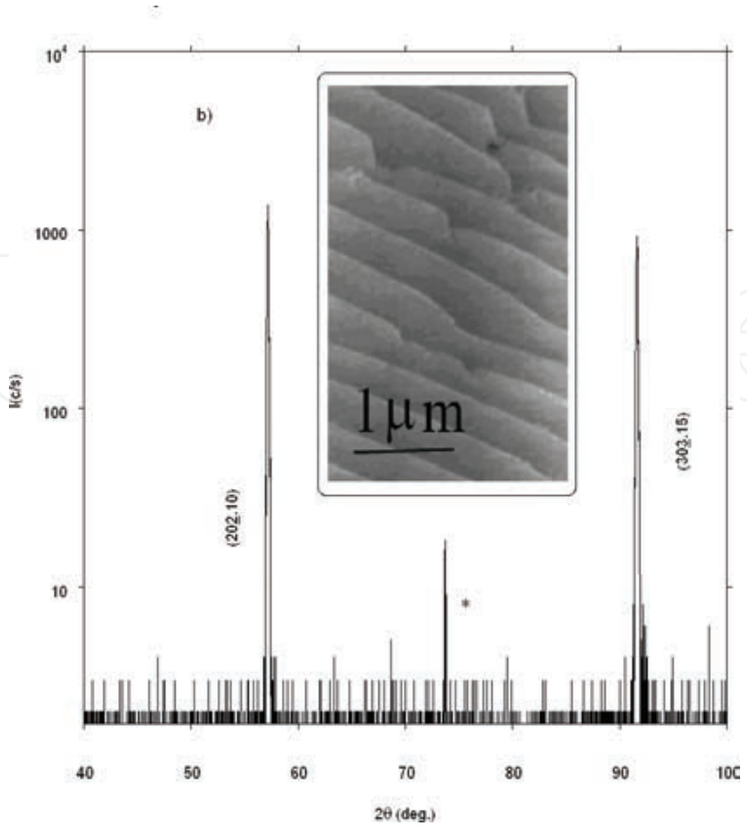

Figure 2. X-ray ω/2Θ scan traced for the grown $Bi_{0.5}Sb_{1.5}Te_3$ film when plane including incident and reflected Roentgen beams was normal to (101.5) plane of the thermoelectric layer. AFM image of free surface of the grown thermoelectric layer is shown on insert.

3. Thermoelectric properties

Efficiency of thermoelectric energy conversion is dependent on figure of merit (Z) of the used materials ($Z = S^2 \sigma/\kappa$, where S—Seebeck coefficient, σ—electrical conductivity, and κ—thermal conductivity) with electron and hole conductance. Thermoelectric properties of bismuth telluride and related solid solution $Bi_{0.5}Sb_{1.5}Te_3$ heteroepitaxial nanostructured films were investigated below room temperature. The temperature dependences of the Seebeck coefficient S and the electroconductivity σ of the Bi_2Te_3 and $Bi_{0.5}Sb_{1.5}Te_3$ films are shown in **Figure 3**. The electrical conductivity of bulk samples grows more sharply with temperature decrease for both Bi_2Te_3 and $Bi_{0.5}Sb_{1.5}Te_3$ solid solution than for films (**Figure 3**, curves 6, 8 and 5, 7). The observed decrease in electrical conductivity in the films is related to the influence of scattering on interphase and intercrystallite grain boundaries.

The temperature dependences of the Seebeck coefficient (**Figure 3**), unlike such electrical conductivity dependences, are located higher for films than for bulk Bi_2Te_3 (curves 1, 2) and $Bi_{0.5}Sb_{1.5}Te_3$ (curves 3, 4). The highest power factor values were obtained in submicrometer $Bi_{0.5}Sb_{1.5}Te_3$ film at $S = 242\ \mu V\ K^{-1}$ over the temperature range of 80–300 K and in the $Bi_{0.5}Sb_{1.5}Te_3$ film at $S = 234\ \mu V\ K^{-1}$ over the range of 130–260 K (**Figure 4**, curves 5, 3). An

http://dx.doi.org/10.5772/65750

enhancement of the Seebeck coefficient and change in its temperature dependence slope both indicate the changes of charge carrier scattering mechanisms in grown films [14, 15] compared those to the bulk thermoelectric materials (**Figure 4**, curves 1–5 and curves 6–9).

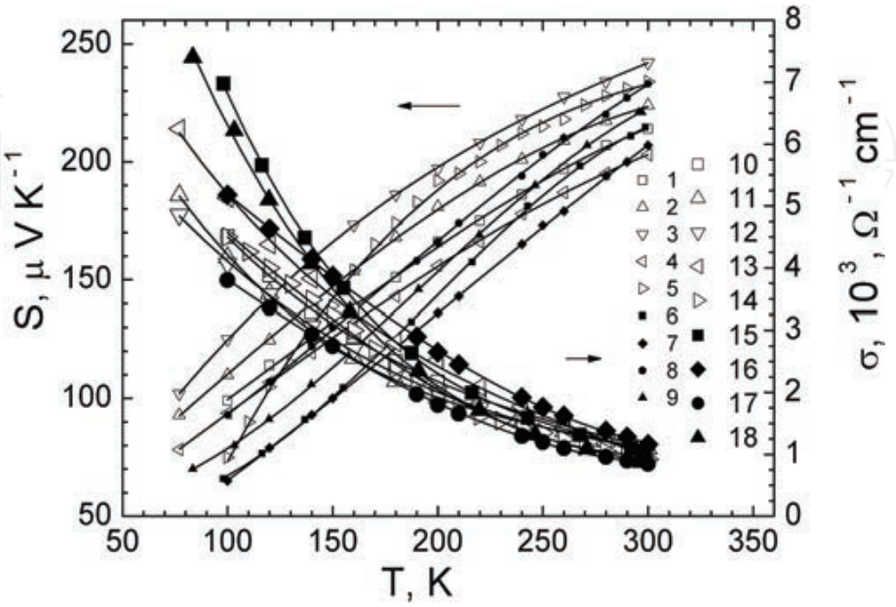

Figure 3. Temperature dependences of the Seebeck coefficient S (1–9), electroconductivity σ (10–18) in heteroepitaxial films (1–5, 10–14), and bulk samples (6–9 and 15–18) of $Bi_{0.5}Sb_{1.5}Te_3$ (1–3, 6–9, 10–12, 16–18) and Bi_2Te_3 (4, 5, 13, 14).

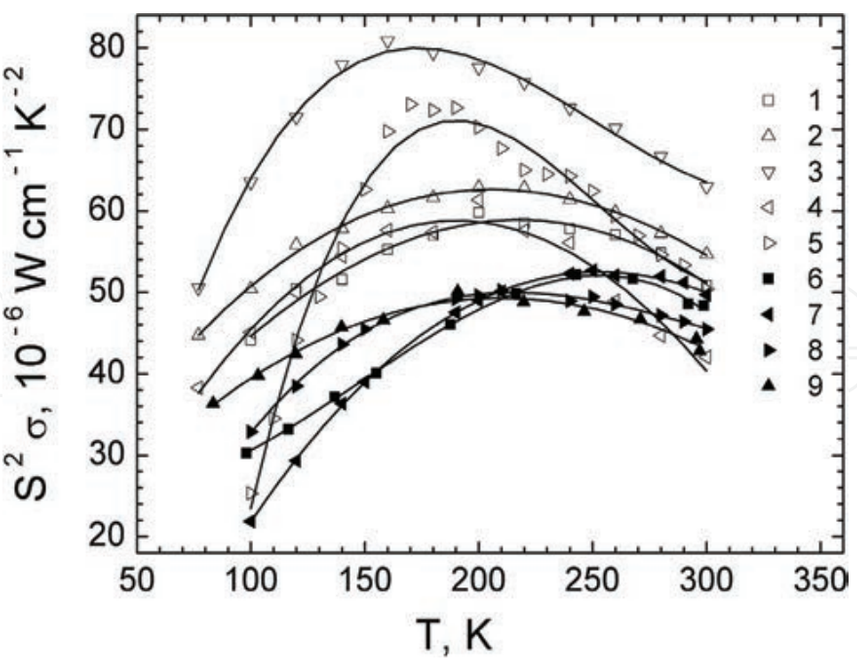

Figure 4. Temperature dependences of power factor $S^2\sigma$ for heteroepitaxial films (1–5) and bulk samples (6–9) of $Bi_{0.5}Sb_{1.5}Te_3$ (1–3, 6–9) and Bi_2Te_3 (4, 5) for S ($\mu V\ K^{-1}$) at room temperatures: 1—214, 2—224, 3—242, 4—203, 5—234, 6—214, 7—207, 8—233, 9—221.

The results of the study of galvanomagnetic and thermoelectric properties in epitaxial films have been used to determine the average effective mass of the density of states m/m_0 and mobility μ_0 of charge carriers taking into account the effective scattering parameter in the model with an isotropic relaxation time similar to the bulk thermoelectrics [14, 16, 17]. Calculations of the effective mass m/m_0 and mobility m_0 have showed that the effective mass of the films is higher than in the bulk samples (**Figure 5**, curves 1–5 and 6, 7) with slight reduction of the mobility in the films (**Figure 5**, curves 13, 14). From the study of the galvanomagnetic properties, the behavior of the effective mass and mobility in the films was found to depend on the scattering mechanism of charge carriers and the parameters of the ellipsoidal constant energy surfaces [13, 18].

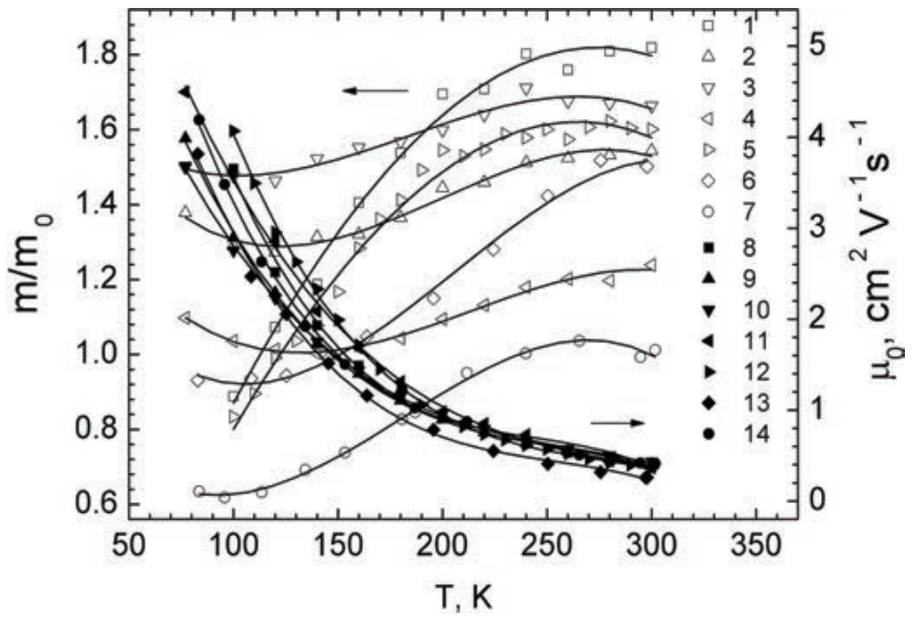

Figure 5. Temperature dependences of the density-of-states effective mass m/m_0 (1–7) and charge carrier mobilitym_0 (8–14) for films (1–5, 8–12) and bulk samples (6, 7, 13, 14) of $Bi_{0.5}Sb_{1.5}Te_3$ (1–3, 6–7, 8–10, 13–14) and Bi_2Te_3 (4, 5, 11, 12).

The product $(m/m_0)^{3/2}\mu_0$, proportional to the figure of merit Z, is higher for films than bulk thermoelectrics due to growth of the effective mass of the density states, which determines an increase in power factor of the films (**Figure 6**). At temperatures below 200 K, an increase in the $(m/m_0)^{3/2}\mu_0$ was observed in the solid solution $Bi_{0.5}Sb_{1.5}Te_3$ at a value of the Seebeck coefficient $S = 242\ \mu V\ K^{-1}$ at room temperature (**Figure 6**, curve 3).

An estimated value of the figure of merit Z in heteroepitaxial $Bi_{0.5}Sb_{1.5}Te_3$ film increases to $3.85 \times 10^{-3}\ K^{-1}$ over the temperature range of 180–200 K. Such increase in Z is approximately by 60% compared to conventional bulk materials and by 20% compared with multicomponent bulk thermoelectrics optimized for temperatures below 200 K [19, 20]. Reduction in thermal conductivity in the $Bi_{0.5}Sb_{1.5}Te_3$ films can reach 20–30% due to additional scattering of charge carriers in the intercrystallite and interphase boundaries [3, 21] that give an additional rise in the figure of merit.

http://dx.doi.org/10.5772/65750

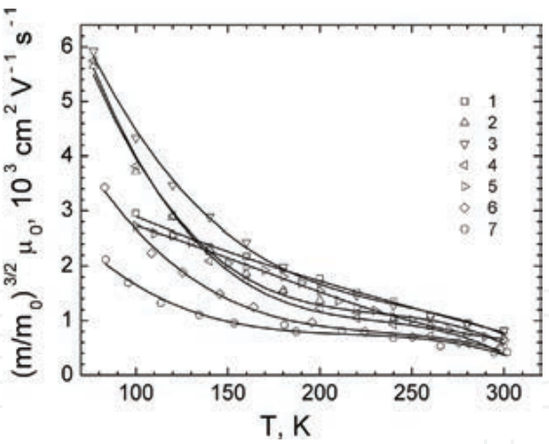

Figure 6. Temperature dependence of the $(m/m_0)^{3/2}\ \mu_0$ parameter for films (1–5) and bulk samples (6, 7) of $Bi_{0.5}Sb_{1.5}Te_3$ (1–3, 5–7) and Bi_2Te_3 (4).

4. Mechanisms of charge carriers scattering

The charge carrier scattering mechanisms of Bi_2Te_3 and solid solution $Bi_{0.5}Sb_{1.5}Te_3$ films were investigated from analysis of the galvanomagnetic coefficients including transverse and longitudinal components of magnetoresistivity tensor r_{ijkl}, electroresistivity r_{ij}, and Hall coefficient r_{ijk} within many-valley model of energy spectrum for isotropic scattering mechanism [14, 18, 22]. A relaxation time for isotropic carrier scattering depends on energy E by power law: $\tau = \tau_0 E^r$, where τ_0 is an energy independent factor and r is the scattering parameter. The least square analysis of experimental galvanomagnetic coefficients for isotropic scattering mechanism permits to determine the degeneracy parameter β_d [13, 15]. The dependence of β_d on temperature obtained in magnetic field at B = 10 T is in agreement with that at B = 14 T (**Figure 7**, curves 1, 2).

The parameter β_d depends on temperature more sharply in the film than in the bulk $Bi_{2-x}Sb_xTe_3$ solid solutions (**Figure 7**, points 3, 4). The temperature dependence of the β_d of the films is supposed to be explained by an additional charge carrier scattering on interphase and intercrystallite boundaries of monocrystalline grains of the films. As shown in **Figure 8**, the dependence of the degeneracy parameter β_d on the reduced Fermi level η shows that the β_d values in films are less than in bulk materials. Therefore, the degeneracy of films is smaller than bulk thermoelectrics [13].

The effective scattering parameter r_{eff} and the reduced Fermi level η were calculated by Nelder-Mead least square method from the temperature dependences of the degeneracy parameter β_d and the Seebeck coefficient S [14, 24]. As compared to bulk materials, the values of the parameter r_{eff} are considerably different from the value r = -0.5, specific for an acoustic phonon scattering mechanism due to sharper energy dependence of electron relaxation time in the films, that is, explained by an additional charge carriers scattering on interphase and intercrystallite boundaries of epitaxial films (**Figure 8**).

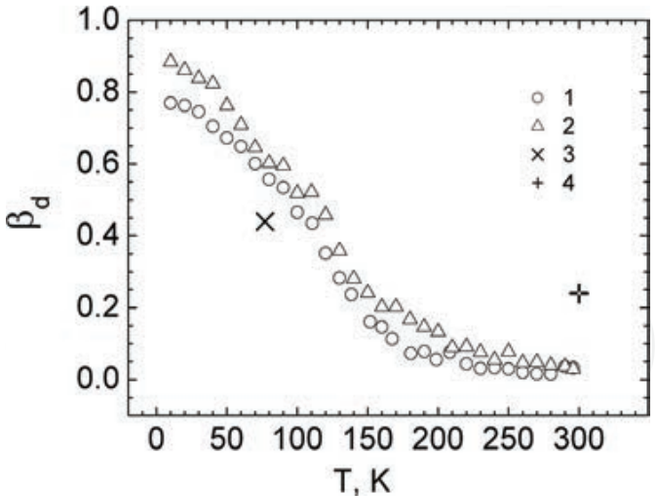

Figure 7. Temperature dependence of the degeneracy parameter β_d (1–2) in the $Bi_{0.5}Sb_{1.5}Te_3$ film. β_d is (1) 10 T and (2) 14 T. Points for bulk solid solutions: 3 [23], 4 [14].

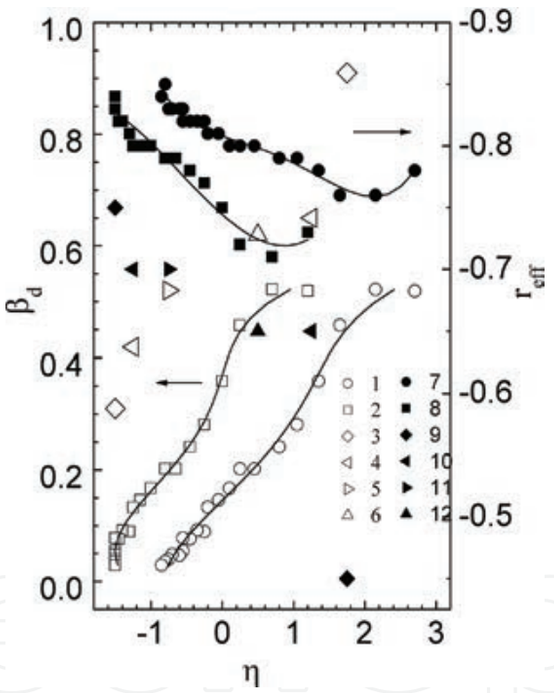

Figure 8. The degeneracy parameter β_d (1–6) and the effective scattering parameter r_{eff} (7–12) on reduced Fermi level η in Bi_2Te_3 (1, 7), $Bi_{0.5}Sb_{1.5}Te_3$ (2, 8) films, and $Bi_{2-x}Sb_xTe_{3-y}Se_y$ (x = 1.2, y = 0.09), (3, 4, 9, 10); $Bi_{2-x}Sb_xTe_{3-y}Se_y$ (x = 1.3, y = 0.07), (5, 11); $Bi_{2-x}Sb_xTe_3$ (x = 1.6), (6, 12) bulk solid solutions.

The materials under study exhibit both anisotropy of the transport properties and anisotropy of charge carrier scattering. In a six-valley model of the energy spectrum with anisotropic scattering of charge carriers, the components of the relaxation time tensor $\overleftrightarrow{\tau}(\varepsilon)$ can be presented as $\tau_{ij} = \varphi(\varepsilon)\tilde{\tau}_{ij}$ where φ(ε) is an isotropic function depending on μ and τ_{ij} is an anisotropic multiplier that is independent on energy. The ratios of the $\overleftrightarrow{\tau}(\varepsilon)$ tensor components

http://dx.doi.org/10.5772/65750

were determined in the temperature interval from 10 to 300 K [15, 17, 25, 26]. The relation between the $\overleftrightarrow{\tau}(\varepsilon)$ components was found as follows: $\tau_{22} > \tau_{11} > \tau_{33}$, and charge carrier scattering along bisector directions was dominant in the film as in the bulk thermoelectrics at low temperatures [17, 25, 27]. The ratio τ_{22}/τ_{11} in the $Bi_{2-x}Sb_xTe_3$ film is increased along bisector axes, but the ratio τ_{33}/τ_{11} is diminished along the trigonal direction in contrast to corresponding bulk thermoelectrics at low [17, 25] and room [27] temperatures. The value τ_{23} is near the same as τ_{11} for the films, while for bulk materials τ_{23} is less than τ_{11}. These specific features of charge carriers scattering lead to increase in the slope of the Seebeck coefficient dependence on temperature (**Figure 3**) and to enhance the thermoelectric power factor for films. Optimization of structure and charge state of the grains and/or interface boundaries might be in favor of a large thermoelectric power factor and figure of merit.

5. Thermoelectric properties under high pressure

The thermoelectric properties of *n*-$Bi_2Te_{3-x-y}Se_xS_y$ solid solutions with atomic substitutions in the tellurium sublattice at ($x = 0.27$, 0.3, $y = 0$, and $x = y = 0.09$) and p-Bi_2Te_3 were studied under pressure of 8 GPa on submicron layer samples at room temperature using the technique described in Ref. [28–30]. It was found that the Seebeck coefficient decreases and the electroconductivity increases with increasein pressure, but the power factor $S^2\sigma$ increases for all compositions, and becomes maximum at pressures of 3–4 GPa (**Figure 9**). The effective mass m/m_0 and mobility μ_0 in the *n*-$Bi_2Te_{3-x-y}Se_xS_y$ and p-Bi_2Te_3 films were obtained taking into account of the change in the scattering mechanism depending on the solid solution composition and carrier density [14, 31]. With increasing pressure *P*, the effective mass m/m_0 [29] in the n- and p-type compositions decreases (**Figure 10**). For *p*-Bi_2Te_3 and for composition at x = y = 0.09, the dependence of m/m_0 and μ_0 on *P* has an inflection at pressures about 3–4 GPa [29, 30]. These inflections in the dependences of m/m_0 and μ_0 on *P*, observed at nearly the same pressure as for the maximum value of power factor $S^2\sigma$, were explained by the influence of topological phase transition at room temperature (**Figure 10**, curves 3, 7).

The existence of the topological transition in Bi_2Te_3 is confirmed by precise diffraction studies of the pressure dependence of lattice parameters [32], abrupt change in the elasticity modulus and its derivative [33], and the change in the Fermi surface section from study of de Haas-van Alphen [32, 34]. This topological transition in Bi_2Te_3 was also confirmed by study of Raman spectroscopy under high pressure [35]. The maximum of the product $(m/m_0)^{3/2}\mu_0$, proportional to the figure of merit, was observed at about the same pressure range as for the topological transition (**Figure 11**). The estimations of the thermal conductivity κ in the *n*- and *p*-type materials show that increase in κ in the pressure range ~3–4 GPa is not higher than 50% [36]. But the power factor of *n*-$Bi_2Te_{3-x-y}Se_xS_y$ solid solutions and the p-type compositions $Bi_{2-x}Sb_xTe_3$ [29] increases under pressure more significantly, and thus, enhancement of the figure of merit values can reach 50–70% taking into account the influence of topological transition at room temperature.

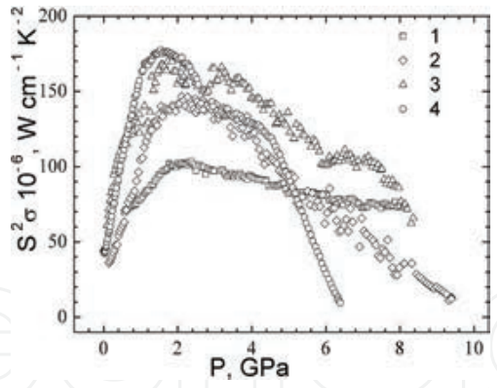

Figure 9. Pressure dependences of power factor of the *n*-$Bi_2Te_{3-x-y}Se_xS_y$ solid solution layers; *x*, *y* are (1) 0.27, 0; (2) 0.3, 0; (3) 0.09, 0.09 and p-Bi_2Te_3 (4).

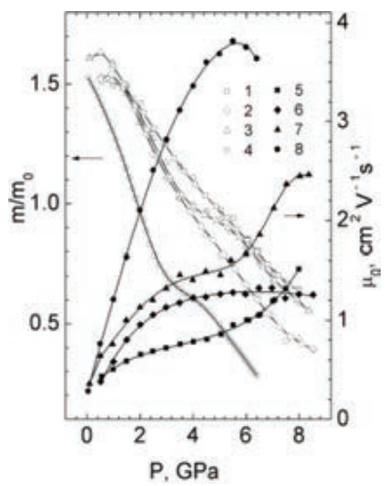

Figure 10. Pressure dependences of the effective mass m/m_0 and the mobility μ_0 of the *n*-$Bi_2Te_{3-x-y}Se_xS_y$ solid solutions; *x*, *y* are (1, 5) 0.27, 0; (2, 6) 0.3, 0; (3, 7) 0.09, 0.09 and p-Bi_2Te_3 (4, 8).

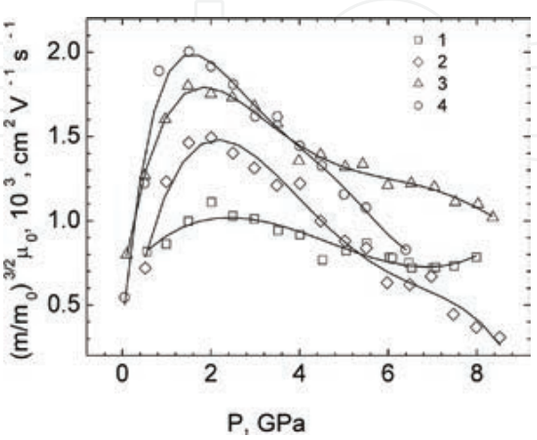

Figure 11. Pressure dependences of the product $(m/m_0)^{3/2}\mu_0$ of the *n*-$Bi_2Te_{3-x-y}Se_xS_y$ solid solutions; *x*, *y* are (1) 0.27, 0; (2) 0.3, 0; (3) 0.09, 0.09 and p-Bi_2Te_3 (4).

http://dx.doi.org/10.5772/65750

6. Quantum oscillations of magnetoresistance

Quantum oscillations of the magnetoresistance associated with surface electronic states in three-dimensional topological insulators have been studied in *p*-type Bi_2Te_3 films [37] in strong magnetic fields from 6 to 14 T at low temperatures (**Figure 12**). The main parameters of surface charge carriers in the films (**Tables 1** and **2**) were determined by analyzing the temperature dependences of normalized amplitude of magnetoresistance oscillations [38]. The phase shift of oscillation period, evaluated by extrapolation of dependence of the Landau level indexes (n = 2, 3, 4, 5) (**Figure 12**) on inverse magnetic field in the limit of 1/B = 0, was found to be consistent with the value of π Berry phase, which is characteristic of surface states of Dirac fermions with linear dispersion [37]. The obtained parameters of the surface states of charge carriers in the nanostructured materials under consideration are important for the development of new high-performance thermoelectrics. The parameters of the surface states of Dirac fermions, such as the mean free path and the energy dependence of lifetime of the charge carriers at the surface, the Fermi energy and respective position of the Fermi level, have a specific influence on the Seebeck coefficient and power factor.

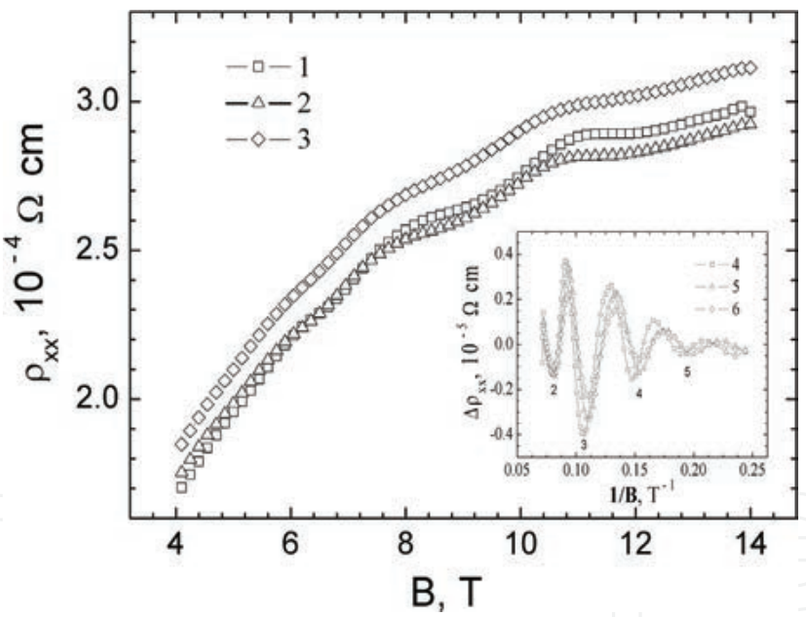

Figure 12. Magnetoresistance dependence ϱ_{xx} (1–3) on magnetic field B and quantum oscillations $\Delta\varrho_{xx}$(4–6) dependence on inverse magnetic field 1/B; ϱ_{xx} at the temperatures: 1, 4–1.6 K, 2, 5–4.2 K, 3, 6–10 K and the Landau level index (*n* = 2, 3, 4, 5) corresponding to the minimum amplitudes of the oscillations.

v, THz	v_F, 10^5, m/s	E_F, meV	μ, m^2/Vs	l_F, nm	τ, 10^{-13}, s	T_D, K
2.0	1.06	19.3	0.33	59	5.5	2.2

Table 1. Cyclotron resonance frequency ν, Fermi velocity v_F, Fermi energy E_F, charge carrier mobility μ, mean free path of charge carriers l_F, the relaxation time τ, and Dingle temperature T_D of the Bi_2Te_3 films.

F, T	$S(k_F)$, nm^{-2}	k_F, nm	$n_{Fs} \times 10^{12}$, cm^{-2}
24	0.23	0.27	0.58
30 [39]	0.29	0.30	0.72
41.7 [40]	0.40	0.36	1.0
50 [39]	0.48	0.39	1.21

Table 2. Frequency of quantum oscillations of the magnetoresistance F, cross section of the Fermi surface $S(k_F)$, Fermi wave vector k_F, and surface concentration of charge carriers n_{Fs} in the Bi_2Te_3 films.

7. Raman spectra

The resonance Raman scattering and morphology of an interlayer van der Waals surface (0001) in thin layer films of chalcogenides based on bismuth and antimony were studied in dependence on the composition, the Seebeck coefficient, and the thickness of the samples. Raman spectra of optical phonons E_g^2, A_{1u}^2, and A_{1g}^2 in thin layers of binary compound n-Bi_2Te_3 and alloys $Bi_2Te_{3-y}Se_y$, $Bi_{2-x}Sb_xTe_{3-y}Se_y$, in heteroepitaxial films of p-Bi_2Te_3 and chemically foliated solid solutions $Bi_{2-x}Sb_xTe_{3-y}Se_y$ are shown in **Figures 13** and **14**. The morphology of the interlayer surfaces (0001) of these samples was studied by atomic force microscopy.

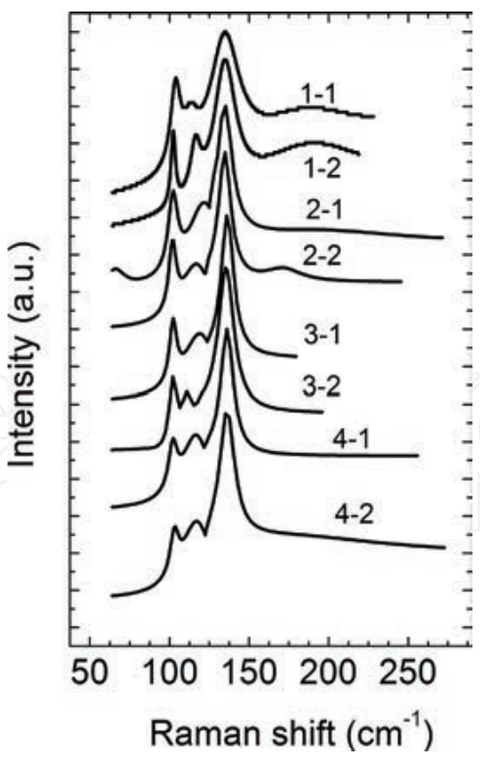

Figure 13. Raman spectra of mechanically split thin layers of n-Bi_2Te_3 (1-1, 1-2), n-$Bi_2Te_{2.88}Se_{0.12}$ (2-1, 2-2) and n-$Bi_2Te_{2.7}Se_{0.3}$ (3-1, 3-2, 4-1, 4-2). (1-1, 1-2): S = -270 μV K^{-1}, R_q = 0.45 nm, H_a = 1.75 nm. (2-1, 2-2): S = -285 μV K^{-1}, R_q = 3.8 nm, H_a = 8 nm. (3-1, 3-2): S = -305 μV K^{-1}, R_q = 4.6 nm, H_a = 15 nm. (4-1, 4-2): S = -315 μV K^{-1}, R_q = 2.9 nm, H_a = 2.3 nm.

http://dx.doi.org/10.5772/65750

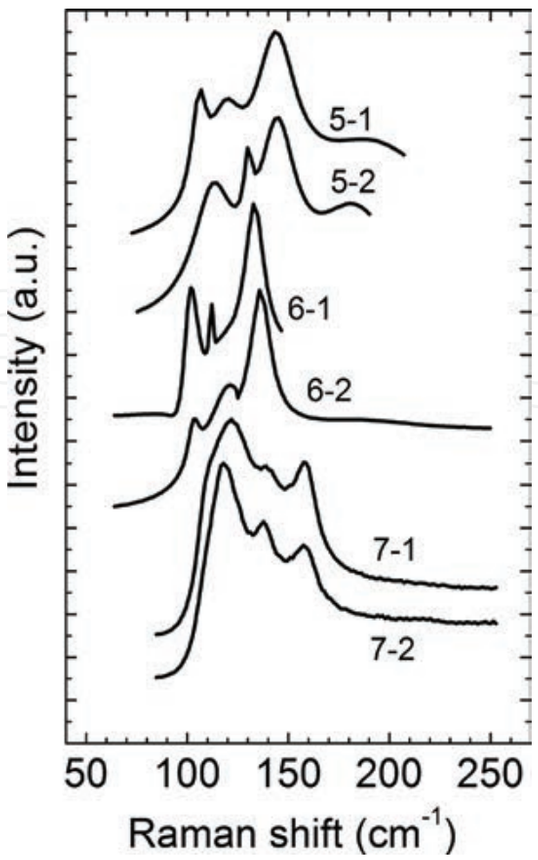

Figure 14. Raman spectra of the thin films of n-$Bi_{1.6}Sb_{0.4}Te_{2.91}Se_{0.09}$ (5-1, 5-2), p-Bi_2Te_3 (6-1, 6-2) and foliated $Bi_{0.9}Sb_{1.1}Te_{2.94}Se_{0.06}$ (7-1, 7-2) solid solution. (5-1, 5-2): S = -280 μV K^{-1}, R_q = 0.36 nm, H_a = 1.55 nm. (6-1, 6-2): R_q = 0.56 nm, H_a = 1.8 nm. (7-1, 7-2): S = -280 μV K^{-1}. (7-1) dissolution time t = 150 h, R_q = 36 nm, H_a = 180 nm. (7-2) t = 200 h, R_q = 26 nm, H_a = 80 nm.

The roughness R_q and H_a corresponding to the maximum of the distribution function of nanofragment heights on the surface of samples [41] are indicated in the captions of **Figures 13** and **14**.

The appearance of the inactive phonons A_{1u}^2 in the Raman spectra, caused by a violation of the inversion symmetry of the crystal, was revealed at decreasing sample thickness and also at high pressure for which topological phase transition in Bi_2Te_3 [35] was observed. Therefore, the occurrence of the A_{1u}^2 was explained by the behavior of surface electronic states of Dirac fermions [42, 43]. The relative intensities $I(A_{1u}^2)/I(E_g^2)$ have maximal values in the most thin layers of solid solutions of n-$Bi_2Te_{2.7}Se_{0.3}$, n-$Bi_{1.6}Sb_{0.4}Te_{2.91}Se_{0.09}$, and epitaxial film of the p-B_2Te_3 with high Seebeck coefficients (**Figure 15**) with high quality of the interlayer (0001) surface with small roughness R_q and H_a values (**Figures 13** and **14**). In the samples n-$Bi_2Te_{2.88}Se_{0.12}$, prepared by the Czochralski technique and by the chemical foliated p-$Bi_{0.9}Sb_{1.1}Te_{2.94}S_{0.06}$ the ratio $I(A_{1u}^2)/I(E_{g2})$, is quite lower (**Figure 15**, curves 2, 7). So the ratio $I(A_{1u}^2)/I(E_{g2})$ is strongly affected by the used technology, composition and thickness of the samples. The analysis of the Raman spectra of bismuth telluride and its solid solutions allows to optimize the Seebeck coefficients, composition, sample thickness, and morphology of the surface, which provide the significant role of surface states of Dirac fermions at room temperature.

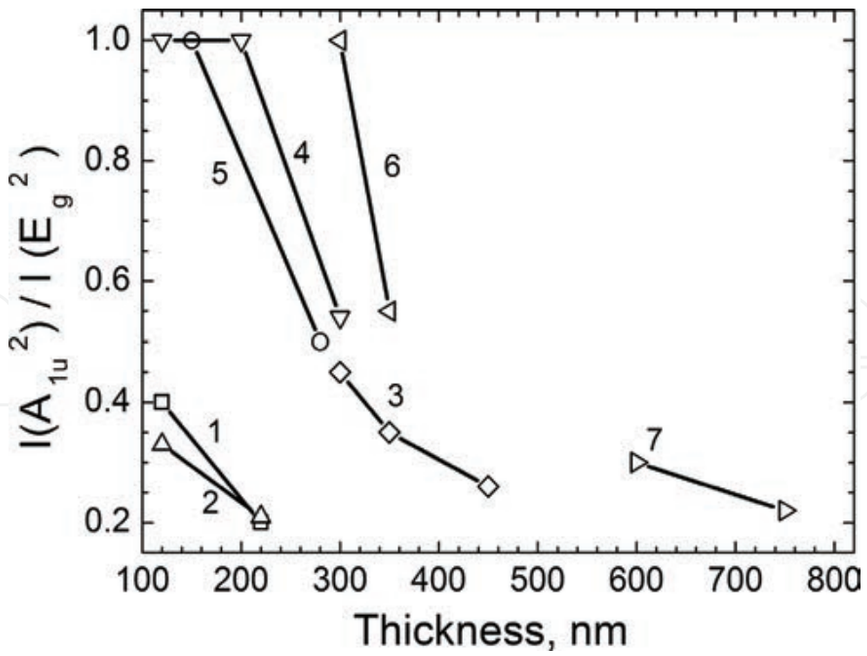

Figure 15. The dependence of the relative intensities $I(A_{1u}^2)/I(E_g^2)$ on the thickness of the layers of n-Bi_2Te_3 (1), n-$Bi_2Te_{2.88}Se_{0.12}$ (2), n-$Bi_2Te_{2.7}Se_{0.3}$ (3, 4), n-$Bi_{1.6}Sb_{0.4}Te_{2.91}Se_{0.09}$ (5), p-Bi_2Te_3 (6), and p-$Bi_{0.9}Sb_{1.1}Te_{2.94}Se_{0.06}$ (7).

8. Conclusion

The thermoelectric and galvanomagnetic properties of heteroepitaxial films based on bismuth telluride, grown by the hot wall epitaxy method, were investigated. The highest power factor was obtained in the $Bi_{0.5}Sb_{1.5}Te_3$ films. An enhancement of the Seebeck coefficient and change in its temperature dependence slope both indicate the variation in the charge carrier scattering mechanisms compared to the bulk thermoelectric materials. The increase in the power factor and $(m/m_0)^{3/2}\mu_0$, associated with the increase in the effective mass of density of states m/m_0, and the reduction in thermal conductivity lead to an increase in the figure of merit Z in the $Bi_{0.5}Sb_{1.5}Te_3$ films up to 3.85×10^{-3} K^{-1} over the temperature range of 180–200 K. Such increase in Z is approximately more by 60% compared to similar bulk materials. The charge carrier scattering mechanisms of the $Bi_{0.5}Sb_{1.5}Te_3$ films were investigated from the data on galvanomagnetic properties for isotropic and anisotropic scattering within many-valley model of energy spectrum. For isotropic scattering, the degeneracy parameter β_d, the effective scattering parameter r_{eff}, and the reduced Fermi level η were calculated. As compared to bulk materials, the values of the parameter r_{eff} are considerably different from r = -0.5, specific for an acoustic phonon scattering in the epitaxial films. The difference of the r_{eff} values is related to an additional charge carriers scattering on interphase and intercrystallite boundaries in the films.

The account of anisotropy of the carrier scattering mechanism has shown that scattering along bisector crystallographic axes is main as compared with corresponding bulk thermoelectrics. Revealed charge carrier scattering peculiarities affect transport properties of the films and might be in favor of a large thermoelectric power factor and the figure of merit.

http://dx.doi.org/10.5772/65750

The studies of the thermoelectric properties of the n-$Bi_2Te_{3-x-y}Se_xS_y$ solid solutions under pressure have shown the increase in power factor and product $(m/m_0)^{3/2}\mu_0$, which is determined by the growth of the effective mass m/m_0. In the composition *n*-$Bi_2Te_{3-x-y}Se_xS_y$ (x = y = 0.09) and p-Bi_2Te_3, the change in the slopes of the pressure dependence of the effective mass and the mobility in the range of 3–4 GPa are coincident with maximum of power factor and explained by an influence of the topological transition. An increase in the thermoelectric figure of merit, as compared to normal conditions, was estimated as 50–70% under pressure due to effect of the topological transitions.

Quantum oscillations of the magnetoresistance were revealed at low temperatures T below 10 K in the range of magnetic field from 6 to 14 T in nanostructured submicron Bi_2Te_3 films grown by hot wall technique. From the analysis of the magnetoresistance oscillations, the cyclotron resonance frequency, cross-sectional Fermi surface, Landau level indexes and π Berry phase, effective cyclotron mass, Fermi wave vector, velocity and Fermi energy, surface charge carrier concentration, lifetime, and mobility of charge carriers were evaluated. The estimated parameters of topological electronic surface states of nanostructured chalcogenides of bismuth and antimony are of special interest for development of new high-performance thermoelectrics, because the Seebeck coefficient and hence power factor are significantly determined by the basic parameters such as charge carriers lifetime, the mean free path of charge carriers, and Fermi energy level position.

The resonance Raman scattering and morphology of the interlayer surface (0001) of bismuth and antimony chalcogenides were studied at room temperature depending on the composition, the Seebeck coefficient, and the thickness of the layers. Raman shifts and the relative intensities of phonon modes were studied in mechanical and chemical foliated thin layers and epitaxial films of bismuth telluride and its solid solutions. The increase in relative intensity ratio of Raman inactive phonons $I(A_{1u}^2)/I(E_g^2)$, sensitive to the topological surface states, was observed for thin layers of n-$Bi_2Te_{2.7}Se_{0.3}$ and n-$Bi_{1.6}Sb_{0.4}Te_{2.91}Se_{0.09}$ solid solutions at low carrier density with Seebeck coefficient values more than -280 $\mu V\,K^{-1}$ and in epitaxial p-B_2Te_3 film grown by the hot wall method on mica with perfect interlayer surface. Thus, the resonance Raman spectra analysis allows to optimize the composition, thickness, Seebeck coefficient values, and morphology of the layers and films with enhanced contribution of the topological surface states at room temperature, which increases the prospects of application of these thermoelectrics.

Author details

Lidia N. Lukyanova*, Yuri A. Boikov, Oleg A. Usov, Mikhail P. Volkov and Viacheslav A. Danilov

*Address all correspondence to: lidia.lukyanova@mail.ioffe.ru

Ioffe Institute, Saint Petersburg, Russia

References

[1] Rowe DM, editor. Thermoelectrics Handbook: Macro to Nano. CRC Press, Boca Raton; 2006. 954 p. Print ISBN: 978-0-8493-2264-8. eBook ISBN: 978-1-4200-3890-3

[2] Nolas GS, Sharp J, Goldsmid HJ. Thermoelectrics: Basic Principles and New Materials Developments. Springer, New York; 2001. 295 p. ISBN: 978-3-662-04569-5

[3] Rowe DM, editor. Modules, Systems, and Applications in Thermoelectrics. CRC Press, Boca Raton; 2012. 581 p. ISBN: 978-1-4398-7472-1

[4] Hasan MZ, Kane CL. Colloquium: topological insulators. Rev. Mod. Phys. 2010; 82: 3045–67. doi:10.1103/RevModPhys.82.3045

[5] Qu DX, Hor YS, Xiong J, Cava RJ, Ong NP. Quantum oscillations and hall anomaly of surface states in the topological insulator Bi_2Te_3. Science. 2010; 325: 821–4. doi:10.1126/science.1189792

[6] Chen YL, Analytis JG, Chu JH, Liu ZK, Mo SK, Qi XL, Zhang HJ, Lu H, Dai X, Fang Z, Zhang SC, Fisher IR, Hussain Z, Shen ZX. Experimental realization of a three-dimensional topological insulator Bi_2Te_3. Science. 2009; 325: 178–81. doi:10.1126/science.1173034

[7] Seradjeh B, Moore JE, Franz M. Exciton condensation and charge fractionalization in a topological insulator film. Phys. Rev. Lett. 2009; 103: 066402/1–4. doi:10.1103/PhysRevLett.103.066402

[8] Chen Y. Topological Insulator Based Energy Efficient Devices. Proc. SPIE. 2012; 8373: 83730B/1–5. doi:10.1117/12.920513

[9] Eschbach M, Młyńczak E, Keller J, Kemmerer J, Lanais M, Neumann E, Erich C, Gellman M, Gospodarič P, Döring S, Mussler G, Demarina N, Luysberg M, Bihlmayer G, Schäpers T, Plucinski L, Blügel S, Morgenstern M, Schneider CM, Grützmacher D. Realization of a vertical topological p-n junction in epitaxial Sb_2Te_3/Bi_2Te_3 heterostructures. Nat. Commun. 2015; 6: 8816/1–7. doi:10.1038/ncomms9816

[10] Xu Y, Gan Z, Zhang SC. Enhanced thermoelectric performance and anomalous Seebeck effects in topological insulators. Phys. Rev. Lett. 2014; 112: 226801/1–5. doi:10.1103/PhysRevLett.112.226801

[11] Zhang J, Feng X, Xu Y, Guo M, Zhang Z, Ou Y, Feng Y, Li K, Zhang H, Wang L, Chen X, Gan Z, Zhang SC, He K, Ma X, Xue QK, Wang Y. Disentangling the magnetoelectric and thermoelectric transport in topological insulator thin films. Phys. Rev. B. 2015; 91: 075431/1–11. doi:10.1103/PhysRevB.91.075431

[12] Lopes-Otero A. Hot wall epitaxy. Thin Sol. Films. 1978; 49: 3–57. doi:10.1016/0040-6090(78)90309-7

[13] Boikov Yu A, Lukyanova LN, Danilov VA, Volkov MP, Goltsman BM, Kutasov VA. Features of growth and galvanomagnetic properties of the Bi_2Te_3-based epitaxial films. AIP Conf. Proc. 2012; 1449: 107–10. doi:10.1063/1.4731508

[14] Lukyanova LN, Kutasov VA, Popov VV, Konstantinov PP. Galvanomagnetic and thermoelectric properties of p-$Bi_{2-x}Sb_xTe_{3-y}Se_y$ solid solutions at low temperatures (<220 K). Phys. Solid State. 2004; 46: 1404–9. doi:10.1134/1.1788770

[15] Lukyanova LN, Boikov Yu A, Danilov VA, Volkov MP, Kutasov VA. Parameters of the constant-energy surface and features of charge carrier scattering of Bi_2Te_3-based epitaxial films. J. Electron. Mater. 2013; 42: 1796–800. doi:10.1007/s11664-012-2432-8

[16] Lukyanova LN, Kutasov VA, Konstantinov PP, Popov VV. Optimization of Solid Solutions Based on Bismuth and Antimony Chalcogenides above Room Temperature. In: Rowe DM, editor. Modules, Systems, and Applications in Thermoelectrics. CRC Press, Boca Raton; 2012. pp. 7.1–18. ISBN: 978-1-4398-7472-1

[17] Lukyanova LN, Kutasov VA, Popov VV, Konstantinov PP, Fedorov MI. Anisotropic Scattering in the $(Bi, Sb)_2(Te, Se, S)_3$ Solid Solutions. In: Proceedings of the XXV International Conference on Thermoelectric. IEEE, Austria, Vienna; 2006. pp. 496–9. doi:10.1109/ICT.2006.331342

[18] Lukyanova LN, Boikov Yu A, Danilov VA, Usov OA, Volkov MP, Kutasov VA. Thermoelectric and galvanomagnetic properties of bismuth chalcogenide nanostructured heteroepitaxial films. Semicond. Sci. Technol. 2015; 30: 015011–6. doi:10.1088/0268-1242/30/1/015011

[19] Kutasov VA, Lukyanova LN, Vedernikov MV. Shifting the Maximum Figure-of-Merit of $(Bi, Sb)_2(Te, Se)_3$ Thermoelectrics to Lower Temperatures. In: Rowe DM, editor. Thermoelectrics Handbook: Macro to Nano. CRC Press, Boca Raton; 2006. pp. 37.1–18. ISBN: 978-0-8493-2264-8

[20] Lukyanova LN, Kutasov VA, Popov VV, Konstantinov PP. Galvanomagnetic and thermoelectric properties of multicomponent n-type solid solutions based on Bi and Sb chalcogenides. Phys. Solid State. 2006; 48: 647–53. doi:10.1134/S1063783406040068

[21] Boikov Yu A, Gol'tsman BM, Kutasov VA. Structure effect on thermoconductivity of Bi_2Te_3 and $Bi_{0.5}Sb_{1.5}Te_3$ films. Sov. Phys. Solid State. 1978; 20: 757–60.

[22] Lukyanova LN, Kutasov VA, Popov VV, Konstantinov PP. Galvanomagnetic properties of multicomponent solid solutions based on Bi and Sb chalcogenides. In: Proceedings of the IEEE XXIV International Conference on Thermoelectrics, ICT, Clemson University, SC, USA; 2005. pp. 426–9. doi:10.1109/ICT.2005.1519978

[23] Lukyanova LN, Kutasov VA, Konstantinov PP, Popov VV. Features of the behavior of the figure of merit for p-type solid solutions based on bismuth and antimony chalcogenides. J. Electron. Mater. 2010; 39: 2070–3. doi:10.1007/s11664-009-1007-9

[24] Lagarias JC, Reads JA, Wright MN, Wright PE. Convergence properties of the Nelder-Mead simplex method in low dimensions. SIAM J. Optim. 1998; 9: 112–47.

[25] Ashworth HA, Rayne JA, Ure RW. Transport properties of Bi_2Te_3. Phys Rev. B. 1971; 3: 2646–61. doi:10.1103/PhysRevB.3.2646

[26] Lukyanova LN, Kutasov VA, Konstantinov PP, Popov VV. Effect of charge scattering anisotropy on the thermoelectric properties of the $(Bi,Sb)_2(Te,Se,S)_3$ solid solutions. Phys. Solid State. 2008; 50: 597–602. doi:10.1134/S106378340804001X

[27] Testardi LR, Burstein E. Low- and high-field galvanomagnetic properties of *p*-type Bi_2Te_3. Phys. Rev. B. 1972; 6: 460–9. doi:10.1103/PhysRevB.6.460

[28] Ovsyannikov SV, Shchennikov VV. Pressure-tuned colossal improvement of thermoelectric efficiency of PbTe. Appl. Phys. Lett. 2007; 90: 122103/1–3. doi:10.1063/1.2715123

[29] Ovsyannikov SV, Grigoreva YA, Vorontsov GV, Lukyanova LN, Kutasov VA, Shchennikov VV. Thermoelectric properties of p-$Bi_{2-x}Sb_xTe_3$ solid solutions under pressure. Phys. Solid State. 2012; 54: 2/261–6. doi:10.1134/S1063783412020254

[30] Korobeinikov IV, Luk'yanova LN, Vorontsov GV, Shchennikov VV, Kutasov VA. Thermoelectric properties of n-$Bi_2Te_{3-x-y}Se_xS_y$ solid solutions under high pressure. Phys. Solid State. 2014; 56: 263–9. doi:10.1134/S1063783414020152

[31] Lukyanova LN, Kutasov VA, Konstantinov PP. Multicomponent n-$(Bi,Sb)_2(Te,Se,S)_3$ solid solutions with different atomic substitutions in the Bi and Te sublattices. Phys. Solid State. 2008; 50: 2237–44. doi:10.1134/S1063783408120020

[32] Polvani DA, Meng JF, Chandra Shekar NV, Sharp J, Badding JV. Large improvement in thermoelectric properties in pressure-tuned p-type $Sb_{1.5}Bi_{0.5}Te_3$. Chem. Mater. 2001; 13: 2068–71. doi:10.1021/cm000888q

[33] Sologub VV, Shubnikov ML, Itskevich ES, Kashirskaya LM, Parfen'ev RV, Goletskaya AD. Change of Bi,Te, band structure under hydrostatic compression. Sov. Phys. JETP. 1980; 52: 1203–6.

[34] Itskevich E. S., Kashirskaya L. M., Kraidenov V. F. Anomalies in the low-temperature thermoelectric power of p-Bi_2Te_3 and Te associated with topological electronic transitions under pressure. Semiconductors. 1997; 31: 276–278. doi: 10.1134/1.1187126

[35] Ovsyannikov SV, Morozova NV, Korobeinikov IV, Lukyanova LN, Manakov AY, Likhacheva AY, Ancharov AI, Vokhmyanin AP, Berger IF, Usov OA, Kutasov VA, Kulbachinskii VA, Okada T, Shchennikov VV. Enhanced power factor and high-pressure effects in $(Bi,Sb)_2(Te,Se)_3$ thermoelectrics. Appl. Phys. Lett. 2015; 106 14 143901/1–5. doi: 10.1063/1.4916947

[36] Jacobsen MK, Sinogeikin SV, Kumar RS. Cornelius AL High pressure transport characteristics of Bi_2Te_3, Sb_2Te_3, and $BiSbTe_3$ J. Phys. Chem. Solids 2012; 73: 1154–1158. doi: 10.1016/j.jpcs.2012.05.001

[37] Lukyanova LN., Boikov YuA, Danilov VA, Usov OA, Volkov MP, Kutasov VA. Surface States of Charge Carriers in Epitaxial Films of the Topological Insulator Bi_2Te_3. Phys. Solid State. 2014; 56 5 941–947. doi: 10.1134/S1063783414050163

[38] Shoenberg D. Magnetic Oscillations in Metals. Series: Monographs on Physics. Cambridge University Press, Cambridge; 2009 596 p. ISBN: 9780521118781

[39] Taskin A., Ren Z., Sasaki S., Segawa K., Ando Y. Observation of Dirac Holes and Electrons in a Topological Insulator. Phys. Rev. Lett. 2011; 107: 016801/1–4. doi: 10.1103/PhysRevLett.107.016801

[40] Dong-Xia Qu, Hor YS, Xiong J, Cava RJ., Ong NP. Quantum Oscillations and Hall Anomaly of Surface States in the Topological Insulator Bi_2Te_3. Science. 2010; 39: 821-824. doi: 10.1126/science.1189792

[41] Lukyanova LN, Bibik AYu, Aseev VA, Usov OA, Makarenko IV, Petrov VN, Nikonorov NV, Kutasov VA. Surface Morphology and Raman Spectroscopy of Thin Layers of Antimony and Bismuth Chalcogenides Phys. Solid State. 2016; 58 7 1440–7. doi: 10.1134/S1063783416070258

[42] Shahil K M F, Hossain M Z, Teweldebrhan D and Balandin A A. Effect of injection current density on electroluminescence in silicon quantum dot light-emitting diodes. Appl. Phys. Let. 2010; 95: 153103/1–3. doi: 10.1063/1.3248025

[43] Glinka Yu D, Babakiray S, Johnson T A, Lederman D. Thickness tunable quantum interference between surface phonon and Dirac plasmon states in thin films of the topological insulator Bi_2Se_3. J. Phys.: Condens. Matter. 2015; 27: 052203/1–7 doi: 10.1088/0953-8984/27/5/052203

IntechOpen